frontiers | Frontiers in Materials

REVIEW
published: 09 June 2022
doi: 10.3389/fmats.2022.910081

Biomimetic Hierarchical Superstructures: Approaches Using Bicontinuous Microemulsions and Electrodeposition

*Ana Sofia Siller-Martínez[1], Keyla M. Fuentes[2], Elijah T. Adesuji[1,2], Frida Aceves[2], Verónica O. Torres-Guerrero[2,3], Esther Guardado-Villegas[2,4], Karla Basilio-Bernabé[2,5], Manuel Ceballos[2], María Navarro-Segura[2], Rubén Darío Rivera-Rangel[2], J. Alejandro Arizpe-Zapata[2], Marcelo Videa[1] and Margarita Sánchez-Domínguez[2]**

[1]Department of Sciences, School of Engineering and Sciences, Tecnológico de Monterrey, Monterrey, Mexico, [2]Centro de Investigación en Materiales Avanzados, S. C. (CIMAV), Unidad Monterrey, Group of Colloidal and Interfacial Chemistry Applied to Nanomaterials and Formulations, Parque de Investigación e Innovación Tecnológica, Apodaca, Mexico, [3]Universidad Tecnológica de Querétaro, UTEQ, Santiago de Querétaro, Mexico, [4]Universidad Autónoma de Sinaloa, Cd Universitaria, Culiacán Rosales, Mexico, [5]Instituto Tecnológico Superior de Poza Rica, III Ver., Poza Rica de Hidalgo, Mexico

OPEN ACCESS

Edited by:
Jie-Sheng Chen,
Shanghai Jiao Tong University, China

Reviewed by:
Feng Bai,
Henan University, China
Zhen-An Qiao,
Jilin University, China

***Correspondence:**
Margarita Sánchez-Domínguez
margarita.sanchez@cimav.edu.mx

Specialty section:
This article was submitted to Colloidal Materials and Interfaces, a section of the journal Frontiers in Materials

Received: *31 March 2022*
Accepted: *03 May 2022*
Published: *09 June 2022*

Citation:
Siller-Martínez AS, Fuentes KM, Adesuji ET, Aceves F, Torres-Guerrero VO, Guardado-Villegas E, Basilio-Bernabé K, Ceballos M, Navarro-Segura M, Rivera-Rangel RD, Arizpe-Zapata J, Videa M and Sánchez-Domínguez M (2022) Biomimetic Hierarchical Superstructures: Approaches Using Bicontinuous Microemulsions and Electrodeposition. Front. Mater. 9:910081. doi: 10.3389/fmats.2022.910081

The current challenges in developing novel nanotechnological processes have led us to explore new methods for synthesizing nanomaterials whose functionalities rely on their structural complexity. In this respect, nature has always been a source of inspiration for proposing innovative technologies to improve the quality of life. Hierarchical superstructures (HSS) are of great interest because the self-assembly of low-dimensional nanostructures (up to the macroscale) allows the control and optimization of performance by coupling the properties of the individual blocks. Self-assembled surfactant structures are convenient for HSS synthesis because they provide a confined reaction medium which confers excellent control over the size of the building blocks. Furthermore, bicontinuous microemulsions offer a soft three-dimensional template due to their interconnected nature. Similarly, electrodeposition routes offer fast, robust, clean, and reproducible ways to synthesize metallic and multimetallic HSS. The combination of soft-templating and electrodeposition is a powerful tool for controlling the morphology and composition of the material. This work reviews polymeric, ceramic, and metallic hierarchical superstructures synthesized using bicontinuous microemulsions and electrodeposition techniques and compares them with matching natural patterns. The aim is to show how these synthetic routes can be exploited to obtain efficient biomimetic nanomaterials that improve their properties.

Keywords: hierarchical superstructures, biomimetics, bicontinuous microemulsion, self assembly, electrodeposition

INTRODUCTION

Hierarchical superstructures (HSS) are nanometric building blocks that self-assemble to extend into one or more dimensions, with a constant and reproducible architectural design. Arrangement of nanoparticles into higher-order domains allows tuning their magnetic, optical, catalytic, or electronic responses by coupling the properties of individual building blocks (Adesuji et al., 2020a; 2020b).

HSSs are characterized by unique physical and chemical properties depending on their morphological structure; for example, they can have a more effective mass and charge transfer due to their related, interconnected nanostructure and tremendous catalytic performance due to their large surface area (Adesuji et al., 2020b). Hierarchical meso-macroporous materials have the advantage that their constituent blocks provide size and shape selectivity, which has led to several applications involving interactions with host molecules. Macropores favor the diffusion and accessibility of host molecules, while mesopores provide a high surface area to enhance adsorption (Fuentes et al., 2019).

Top-down and bottom-up approaches conduct to 3D-ordered macrostructures such as HSS. However, self-assembly from basic building block units with low dimensionality (i.e., bottom-up approach) allows greater structural control, opening unlimited possibilities concerning the design and construction of functional nanostructured materials. It can be more cost-effective than top-down nanofabrication (Iqbal et al., 2012). Typical examples are SiO_2 and latex spheres ordered as opals. They can be infiltrated with a precursor to obtain reverse opal structures using sol-gel, hydrothermal, or solvothermal approaches (Miguez et al., 1997; Zeng et al., 2002). Another example is using butterfly wings as biotemplates under the same principle (Song et al., 2019). However, this strategy has the disadvantage that chemical and thermal processes are required to remove the template, and in most cases, it can be detrimental to the final structure.

Biological structures presenting a wide variety of growth patterns are formed as a result of the molding processes of surface-active molecules, mainly polymers, and some low-molecular-weight polar lipids (Holmberg, 2004; Amstad and Harrington, 2021). Likewise, the inhibitory and activator coupling reactions between the chemical precursors and their spatially-constrained diffusion, was described by the reaction-diffusion model introduced by A.M. Turing (Turing, 1952). The recognition of the experimental conditions associated with pattern formation has been used extensively in recent decades to rationally synthesize inorganic materials with nanometric dimensions (Judit et al., 2009; Sanchez-Dominguez et al., 2012; Wang et al., 2021). Self-assembled, reaction-confining surfactant systems such as micelles, microemulsions, or liquid crystals can be used as soft templates. Therefore, nanofabrication in surfactants-based systems can be considered a biomimetic approach.

Microemulsions are liquid water-surfactant-oil mixtures structured into separate polar and nonpolar domains with typical length scales between 10 and 400 Å and separated by a monolayer of oriented surfactant molecules (Danielsson and Lindman, 1981; Lindman et al., 1989; Olsson and Lindman, 1990). Remarkably, bicontinuous microemulsions (BμEs) represent an exciting soft template for 3D structures. Interconnected aqueous and oily nanochannels with infinite length characterize these thermodynamically stable colloidal dispersions, capable of conferring great versatility during the synthesis. Nucleation, growth, and self-assembly can occur in a single step because they act as nano-confined reactors and long-range templates, allowing the formation of HSS, going all the way from the nano to the macroscale (Sims et al., 1998; Latsuzbaia et al., 2015; Galiano et al., 2018; Adesuji et al., 2020b). Moreover, they allow the combination of precursors of different chemical nature because both hydrophilic and lipophilic precursors can be used (Adesuji et al., 2020b). A schematic representation of the template effect of a BμE is presented in **Figure 1**, where the superstructure grows in the aqueous or oil phase, depending on the solubility and hence the location of the chemical precursors. When the reagents are incorporated, they may react either in the aqueous phase, in the oil phase, or at the oil/water interface. Then, the formed nanoparticles grow and self-assemble inside the nanochannels, to be finally recovered from the liquid microemulsion medium by physical means.

On the other hand, electrodeposition is an economical and environmentally friendly process due to its lower operating temperature and pressure requirements, more accessible instrumentation, and high-quality deposits. Controlling the chemical composition and deposition properties by manipulating the electrodeposition parameters is another advantage of this technique (Omar, 2021). Additionally, surface morphology and surface composition in electrochemical systems can couple to induce Turing pattern formation in electrodeposits due to the feedback between the reaction dynamics and the electrode's double layer potential (Dobrovolska et al., 2012; Sgura et al., 2019). Metallic or multimetallic HSS can be obtained via electrodeposition. For instance, certain porous materials, such as anodized aluminum oxide or copper membranes, are common hard templates for electrodeposited nanotubes or nanowires (Strukov and Strukova, 2013; Kawamura et al., 2014). Soft templating in electrochemical-based synthesis has been explored in several materials as an improved method for obtaining 3D-ordered catalysts (Attard et al., 1997; Zhu et al., 2015; Li et al., 2018; Shi et al., 2021; Zhang et al., 2021; Fradin et al., 2022).

Similarly, nature takes advantage of the structural characteristics to adapt and improve the intrinsic properties of biomaterials and minerals. During long-term evolution, many species have developed superstructures that modify, optimize, and adjust to the material's intrinsic properties that characterize them. Some examples are (*i*) the structural colors of fungi, birds, or insects (butterfly wings) (Mason, 1926, 1927; Brodie et al., 2021), (*ii*) the collagen fiber formed by amino acids self-assembled as a triple helix (Mercatelli et al., 2019), and (*iii*) the silica shell (frustule) of diatoms that exhibits intricate geometric characteristics at the micro and nanoscale (Belegratis et al., 2013). Thus, understanding the underlying complex, non-linear mechanisms of self-organization present in biological systems is of great interest in preparing novel bio-inspired and biomimetic materials with efficient functionalities for different nanotechnological applications.

This study presents several biomimetic materials in which BμE are used as a soft template. The selected structures were classified according to their chemical nature and compared to their natural patterns. Moreover, some electrodeposited materials highlight the benefits of using electrochemical reactions as clean and fast reaction strategies. Furthermore, electrodeposition with soft templating using bicontinuous microemulsions is discussed as

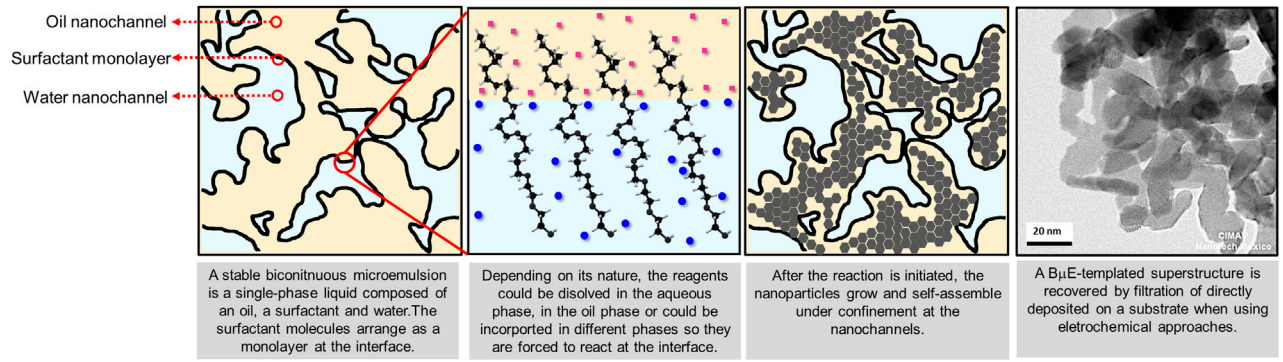

FIGURE 1 | Schematic representation of the template effect of a BμE. A surfactant monolayer separates the water and oil nanochannels. Depending on their chemical nature, the reagents may be incorporated in different combinations (aqueous phase, oil phase, or both). The final HSS can be quickly recovered from the liquid medium.

a potential novel synthetic approach for developing biomimetic HSS.

SYNTHESIS OF HSS USING BICONTINUOUS MICROEMULSIONS

Polymeric HSS

Nanoporous materials are commonly used for storage, catalysis, drug delivery, and as templates for synthesizing nanostructures with specific dimensions, morphologies, and properties. Polymeric HSSs serve as continuous three-dimensional (3D) porous networks. **Figure 2A** shows a transparent nanostructured polymeric bicontinuous material composed of methyl methacrylate (PMMA) and DTAB (n-dodecyltrimethylammonium bromide (CH_2=CHCOO$(CH_2)_{11}N^+(CH_3)_3Br^-$) with the incorporation of an electrolyte (NaCl). The MMA monomer functioned as the oil phase, whereas DTAB worked as a surfactant (Chew et al., 1998). The monophasic region MMA/DTAB was mixed using a vortex. DMPA (2,2-dimethoxy-2-phenylacetophenone) was then added as a photoinitiator; the reaction was conducted in a Rayonet reactor at a wavelength of 253.7 nm for approximately 1 h at 35°C. These materials are reminiscent of the spot patterns of many felines (or other mammals), whose skin is covered with these spots to camouflage themselves in their jungle habitat. These spots are usually produced by mutations in the genes involved in melanin production and have great importance in felines' communication, camouflage, and physiological functions (Guevara-Chumacero, 2006).

Another example of organic materials obtained by polymerization in BμE is presented in **Figure 2B**, which shows a bicontinuous polymeric material consisting of two homopolymers, polyethylene (PE) and polyethylene propylene (PEP), and a symmetrical diblock copolymer PE-PEP, synthesized by Bates et al. (1997). The synthesis of PE-PEP was adapted from a method reported by Rosedale et al. (1995), which begins with the anionic polymerization of poly (1,4-butadiene)- poly(1,4-isoprene) diblock copolymer (1,4PB-1,4PI) as the first step. Then, the resulting copolymer was dissolved in cyclohexane and saturated with hydrogen on a palladium catalyst supported on calcium carbonate close to 70–80°C to obtain the PE-PEP. Swelling increases the space between layers by adding the homopolymer, resulting in a bicontinuous polymeric material (PE-PEP/PE/PEP). These materials recall the patterns formed in human fingertips by the papillary crests (glands for sweat secretion located in the dermis) and increase the contact surface between the dermis and epidermis (Newman, 1944). **Figure 2C** shows a polymeric structure made of nanoporous polyethylene (PE) that resembles the structure of Millipore coral. Jones and Lodge synthesized this material by replicating the inverse structure of a nanoporous material derived from a BμE by nanocasting (Jones and Lodge, 2010). The synthesis required polyethylene (PE) and poly(ethylene-propylene) (PEP) as homopolymers and a symmetrical diblock copolymer of poly(ethylene-block-ethylene-alt-propylene) (PE-PEP), which was synthesized by anionic polymerization, as described previously. Later, to obtain BμE in the solid-state, the crystallization of PE was induced with liquid nitrogen. Finally, the solid monoliths were soaked in THF to remove any remaining homopolymers. In the case of Millepora coral, its calcareous exoskeleton is made up of an inorganic material ($CaCO_3$) deposited by slow crystallization, generation after generation (Le Roy et al., 2021). These examples highlight that one of the most significant advantages of using BμE is the formation of highly cross-linked materials with large surface areas, which is useful for many applications of interest involving mass and charge transfer.

Ceramic HSS

Inorganic materials with modeled architectures are essential because of their great potential in catalysis, membrane and separation technologies, biomaterial science, and sensor devices. The chemical construction of extended microscopic matrices of inorganic materials requires self-organizing systems such as foams. **Figure 3** shows microskeletal calcium

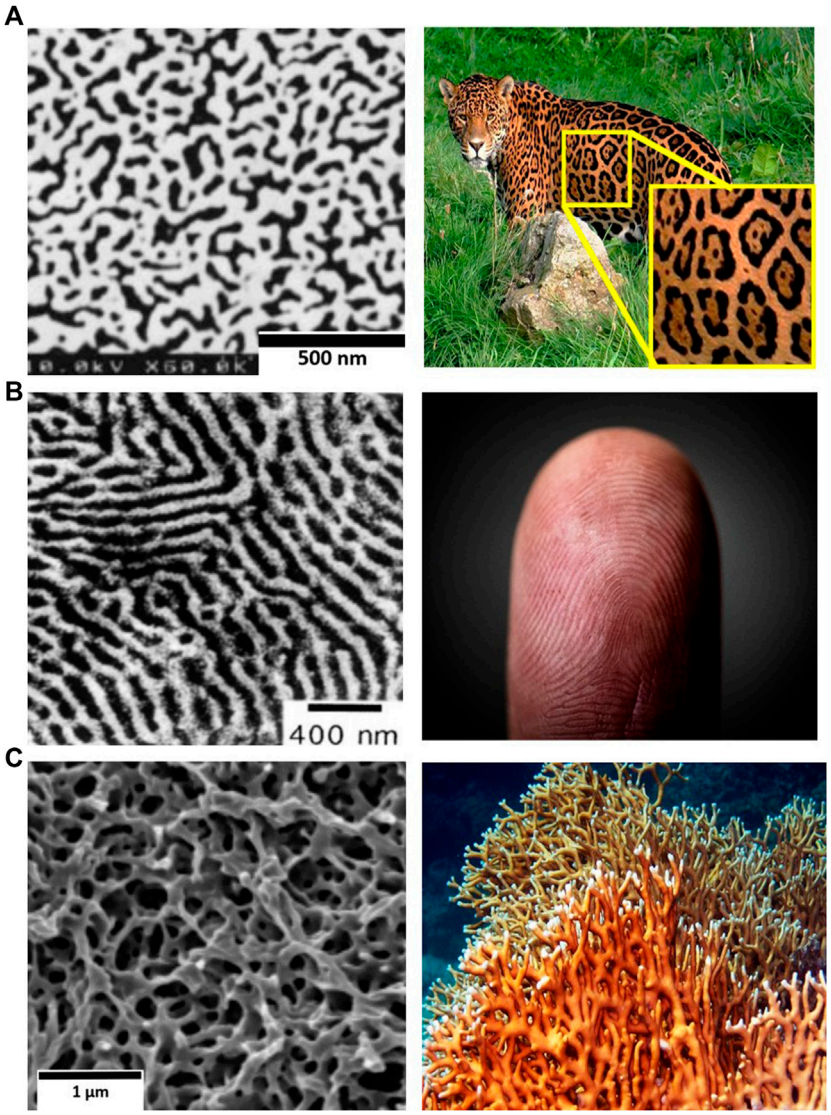

FIGURE 2 | Examples of nanostructured polymeric materials obtained in bicontinuous microemulsion: **(A)** SEM image of transparent nanostructured polymer of MMA/AUTMAB (Reprinted with permission from *Langmuir* 1998, 14, 21, 6068–6076. Copyright (1998) American Chemical Society) Chew et al. (1998) compared to the spot pattern of a feline ("Jaguar" by Chester Zoo is licensed under CC BY-ND 2.0). **(B)** TEM image of the bicontinuous polymeric material of PE-PEP/PE/PEP (Reprinted with permission from *Phys. Rev. Lett.* 79, 849. Copyright (1997) by the American Physical Society), compared with a fingerprint (Copyright: Ivan Radic. Close-up of a fingerprint on a human finger. Available on: https://www.flickr.com/photos/26344495@N05/49463377503. Visited on August 2021). **(C)** SEM image of nanoporous polyethylene (PE) polymeric structure (Reprinted with permission from *Chem. Mater.* 22 (2010) 1279–1281. Copyright (2010) American Chemical Society), compared to the structure of a *Millepora dichotoma* coral (This file is available under the Creative Commons Attribution 2.0 Generic license. Available on: https://es.wikipedia.org/wiki/Millepora#/media/Archivo:Fire_Coral.jpg. Visited on: August 2021).

phosphate crystallized in bicontinuous microemulsions of di-dodecyldimethylammonium bromide (DDAB) and a mixture of tetradecane-hexadecane as the oil phase (Walsh and Mann, 1996). First, a supersaturated (metastable) calcium phosphate solution was prepared with calcium chloride and disodium hydrogen orthophosphate. The microemulsions were then prepared with a supersaturated calcium phosphate solution as the aqueous phase, DDAB as the surfactant, and a tetradecane/hexadecane mixture as the oil phase, which produced a transparent bicontinuous mixture. The mixture was then rapidly frozen by immersion of the vessel into liquid nitrogen, and it was stored at −25°C for up to 21 days to induce crystallization. After centrifugation, the surfactants and residual oils were separated from the mixture, resulting in microskeletal calcium phosphate. The microskeletal structure of this material resembles that of dried luffa (Luffa aegyptiaca). The luffa is a fruit that usually is eaten immature (zucchini), but when ripe, it has a fibrous vascular system similar to a network; it is commonly used as a natural sponge and can be used as an alternative material for artificial cellular materials due to its structure that serves as an open-cell "foam" (Shen et al., 2012).

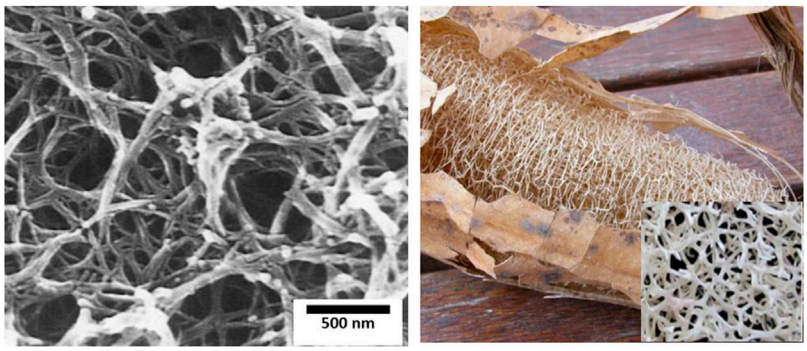

FIGURE 3 | Example of nanostructured ceramic material obtained in bicontinuous microemulsion. SEM of microskeletal calcium phosphate obtained in DDAB bicontinuous microemulsions (Reprinted with permission from *Chem. Mater.* 8 (1996) 1944–1953. Copyright (1996) American Chemical Society) compared with the fibrous structure of the Luffa (Copyright: Martin Stellar/EyeEm. Available on: https://www.gettyimages.fr/detail/photo/high-angle-view-of-dried-loofah-on-table-image-libre-de-droits/649132081. The inset in the figure depicts the microstructure of the luffa fibers (Reprinted from *Materials* 10, 5 (2017) 479. MDPI, Basel, Switzerland under the terms and conditions of the Creative Commons Attribution (CC BY) license).

FIGURE 4 | Examples of ceramic nanostructured meso/macroporous hierarchical spheres. **(A)** TEM of functionalized wrinkled silica spheres with meso/macroporous hierarchical system (Reprinted by permission from J. Porous Mater. 28, 261–269 (2021) Copyright© 2020, Springer Science Business Media, LLC, part of Springer Nature) compared to the Cempasúchil (*Tagetes erecta*) flower (Pixabay license for the public domain. Available on: https://pixabay.com/photos/mexican-marigold-orange-flower-plant-5540037/). **(B)** SEM of meso/macroporous hierarchical SiO_2 spheres decorated with TiO_2NPs (©2019 the chapter is distributed under the Creative Commons Attribution 3.0 License) compared to the *Allium stipitatum* flower (Pixabay license for the public domain. Available on: https://pixabay.com/photos/flowers-ball-of-flowers-white-2628990/).

Porous oxides are significant supports for nanoparticles of catalytic interest, and an adequate porous distribution favors the adsorption and diffusion of the reagents. **Figure 4A** shows amine-functionalized corrugated silica spheres with a hierarchical meso/macroporous system, which have been used to support enzymes of biotechnological interest (Fuentes et al., 2020). Functionalization occurred in the mesopores distributed through the wrinkled walls, and the conservation of

FIGURE 5 | SEM of self-assembled ZnO nanoplatelets prepared using a BµE template (Pemartin, 2013) compared with a desert rose (©2021 CrystalAge.com. Available on: https://www.crystalage.com/online_store/dessert_rose_crystal_specimen_large_858983.cfm).

macropores facilitated the diffusion of enzymes inside the particles. The silica mesostructures were synthesized using a pseudoternary Winsor III microemulsion system (Moon and Lee, 2012). The aqueous phase was a urea solution. The surfactant component was a mixture of cetyltrimethylammonium bromide (CTAB), a quaternary ammonium salt, and 1-butanol (co-surfactant), while the oil phase was cyclohexane. The three components were mixed and stirred vigorously, tetraethyl orthosilicate (TEOS) was added to the emulsion, and maintained stirring. The mixture was heated at 70°C for 19 h. For functionalization, the amino moieties were incorporated through grafting. In this case, although the properties of the reaction medium coincide with those of an emulsion, the corrugated walls and hollow areas have the shape and dimensions expected when using bicontinuous microemulsions. For this reason, it has been proposed that this synthesis occurs in multiple emulsions, where the bicontinuous structure determines the topology of the spheres. In contrast, the size of the emulsion droplet determines the size of the particles. An equivalent to this morphology in nature is the Cempasúchil (*Tagetes erecta*) flower (or Mexican marigold) native to Mexico and characterized by its fractal dimension and coloration due to carotenoids (Quintanilla Carvajal et al., 2015).

The radial growth of corrugated silica (SiO_2) spheres allowed the surface deposition of nanoparticles without losing the internal porosity of the support. This feature is highly desirable in some applications because it provides a high specific surface area and suitable interaction with external parameters, such as radiation. **Figure 4B** shows SiO_2 spheres with hierarchical porosity decorated with TiO_2 nanoparticles (TiO_2NPs) for photocatalytic applications (Fuentes et al., 2019). The SiO_2 corrugated spheres obtained as described previously were decorated by depositing titanium isopropoxide in isopropanol and treated under hydrothermal conditions to achieve the crystallization of TiO_2NPs in the anatase phase with a mean particle size of approximately 10 nm. This distribution allows the semiconductor to interact with incident light at the surface. At the same time, the high porosity of the support favors the adsorption of contaminants, and the size of the SiO_2 spheres allows easy recovery of the reaction medium. These materials remind us of the spherical structure of *Allium stipitatum* flowers, which arise from bulbs or rhizomes, most of which are perennials. The flowers are frequently borne in spherical clusters and produce black seeds in dry capsule fruits (The Editors of Encyclopaedia, 2018).

Another example of ceramic nanostructures is the three-dimensional material obtained by self-assembly of ZnO nanoplates in a bicontinuous microemulsion based on a nonionic surfactant (Pemartin, 2013), where the aqueous phase is composed of a solution of 0.8 M HCl, the surfactant is Synperonic® 10/6, and the oil phase is hexane with zinc 2-ethylhexanoate. The zinc oxide (ZnO) precipitation was induced by adding NaOH to increase the pH within the aqueous nanochannels. Due to the confinement imposed by the nanochannels, one-dimensional (nanowires) structures are initially formed, which then grow further to form nanoplates, followed by their self-assembly into preferential directions to create 3D structures such as desert roses, the remarkable similarity between the two morphologies can be seen in **Figure 5**. These ordered morphologies allow for varying optoelectronic responses of these materials, which can be exploited in applications of great interest, such as gas detection or heterogeneous photocatalysis. Desert roses are sedimentary rocks composed of gypsum ($CaSO_4$), water, and sand formed mainly by precipitation under high evaporation rates (environments like deserts). The crystallization of calcium sulfate by water evaporation occurs in preferential directions, resulting in numerous lenticular crystals intercepting each other (Leblanc, 2019).

Metallic HSS

Metallic materials presenting hierarchical superstructures exhibit increased magnetic, optical, and electronic responses owing to the coupling of the properties of the building blocks. Platinum hierarchical superstructures (PtHSS) shown in **Figure 6A** exhibit improved behavior towards hydrogen evolution reaction by water electrolysis. In addition, Adesuji et al. (2020b), demonstrated that both water-soluble and oil-soluble precursors could be used to synthesize PtHSS, giving a variety of self-assembled structures depending on the phase in which the

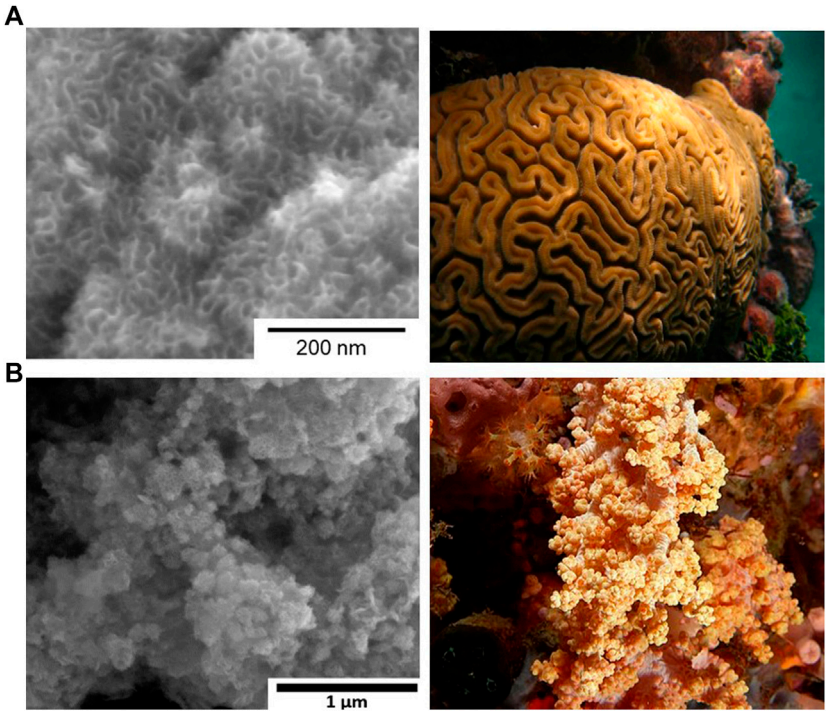

FIGURE 6 | (A) SEM of self-assembled Pt nanoneedles with nanocoral morphology (Reprinted from Electrochim. Acta 354 (2020) 136608. ©2020 Elsevier Ltd. All rights reserved), compared to brain coral *(Diploria labyrinthiformis)* (licensed under Creative Commons 3.0. Available on: https://upload.wikimedia.org/wikipedia/commons/9/92/Mozgovity_koral.jpg). **(B)** SEM of Pt-Co_3O_4 HSS (Reprinted from *Catalysts* 2020, 10 (11), 1311. MDPI, Basel, Switzerland under the terms and conditions of the Creative Commons Attribution (CC BY) license), compared to *Scleronephthya spp*. (Licensed under the Creative Commons Attribution-Share Alike 3.0. Available on: https://upload.wikimedia.org/wikipedia/commons/e/ef/Scleronephthya_sp._%28White_soft_coral_with_apricor_colored_polyps%29.jpg).

reduction reaction occurs (aqueous or oil nanochannels). In this case, a nonionic surfactant (Synperonic^{TM} 91/5) was used, and the oil phase was isooctane. One of the main advantages of the BµE used in this study is their formation at room temperature and the rapid acquisition of highly cross-linked materials. For this procedure, the components were mixed in a vortex, resulting in a transparent, liquid, and isotropic phase, indicating the microemulsion formation. Subsequently, a sodium borohydride solution was added as a reducing agent, and the reaction mixture was stirred in a vortex. Finally, the mixture was maintained at 22°C without stirring overnight. The superstructure obtained when chloroplatinic acid is used (when the precursor is dissolved in the water nanochannels), is formed by the self-assembly of nanoneedles and nanoparticles into spherical assemblies, which are interconnected into a network. This structure resembles an interconnected sponge that can be compared to a brain coral, whose shape could be associated with the infinite aqueous nanochannels of the bicontinuous microemulsion. Crystallization of Pt self-assembled nanoneedles throughout these nanochannels allows the passage from the nano to the macroscale, extending the range of these materials to tens of microns. This self-assembly is extremely important in applications where efficient charge transfer is required, as is the case for water electrolysis to obtain green fuels.

Similarly, the brain coral *(Diploria labyrinthiformis)* or meandroid *(Colpophyllia natans)* forms extensive colonies that can reach more than a meter wide. Its spheroidal and ribbed shape is due to the "self-assembly" of millions of polyp clones covered by a calcareous exoskeleton. The calcareous structure of polyps connects them, creating a colony that functions as an individual organism and whose extended network is vital for the ecosystem because it serves as a refuge for many invertebrate animals and as protection from erosion of the coasts (Torruco Gómez and González Solís, 2011; Coral Reef Alliance, 2021).

Another exciting aspect of bicontinuous microemulsions as nanoreactors is the possibility of combining different metal precursors to obtain multimetallic superstructures and/or hybrid materials. This is of great interest because their performance often exceeds the properties associated with their monometallic counterparts; that is, the physicochemical properties of bimetallic nanomaterials are often better than those of their monometallic counterparts, which is commonly explained as synergistic effects (Notar Francesco et al., 2014). For example, by testing the same microemulsion system as described for platinum in the previous example, the synthesis of a hybrid metal-metal oxide superstructure of Pt-Co_3O_4 was carried out (Adesuji et al., 2020a); the material synthesized by Adesuji *et al.*, is shown in **Figure 6B**. In this case, synthesis by reduction/precipitation occurs in a single step, facilitated by the confined space. The nature of the metallic precursors determines their morphology; thus, water- and oil-soluble Co and Pt precursors were used in different combinations to achieve unique

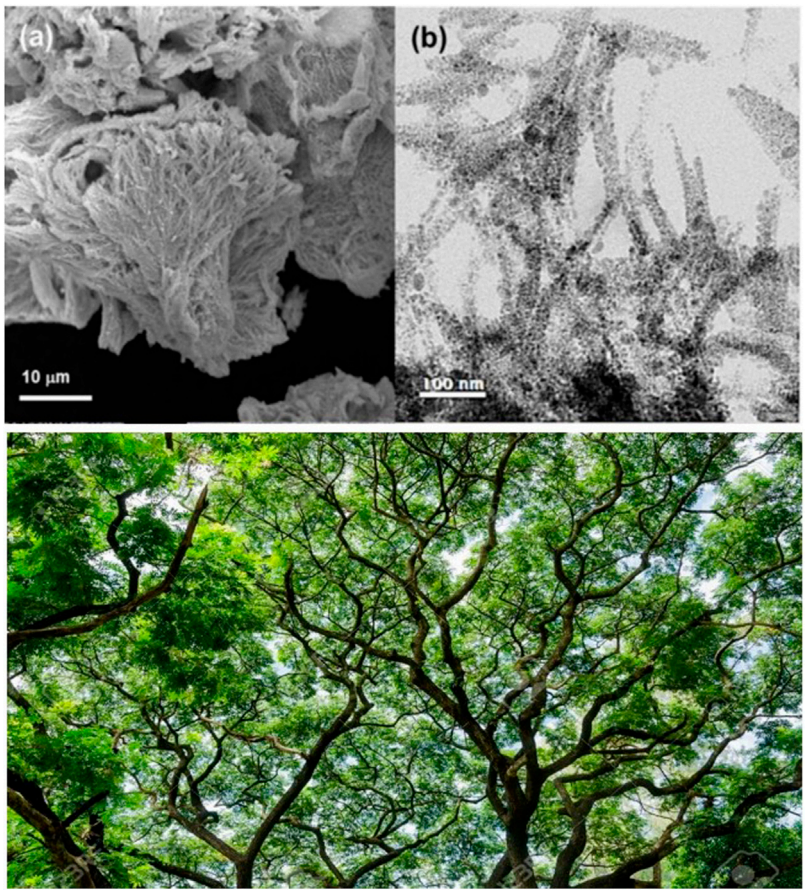

FIGURE 7 | On top are the SEM **(A)** and TEM **(B)** images of the HSS conformed by silver nanoparticles. (Reprinted from Elijah T Adesuji et al. Nanotechnology 31 425601. © 2020 IOP Publishing Ltd.). compared to a photograph of the branches of a tree at the bottom (Copyright: Big trees and branches of trees overhead. Available on: https://www.123rf.com/photo_46784911_big-tree-and-branches-of-tree-over-head.html?vti=o45q22f6rxql0m2okq-1-87.

hierarchical morphologies. The resulting structure of the Pt-Co_3O_4 HSS synthesized with both Pt and Co water-soluble precursors resembles the structure of tree corals (*Scleronephthya spp.*) because of their interconnected needle formation in the form of polyps. *Scleronephthya spp.* is mainly found in the Indo-Pacific region and is characterized by a soft structure, as it does not generate a calcium carbonate skeleton, so they are not reef generators.

As mentioned above, certain properties can be improved when nanoscale building blocks self-assemble into HSS. An example is the formation of self-assembled silver plasmonic nanoparticles, as shown in **Figure 7**. The synthesis of this material is carried out in a bicontinuous microemulsion composed of Synperonic 91/5, isooctane, and water. The ethoxylated groups of the nonionic surfactant reduce the silver ions incorporated into the aqueous phase from the moment the microemulsion is formed (Adesuji et al., 2020c). The size of the plasmonic Ag nanoparticles can be controlled by varying the reaction time. However, these nanoparticles tend to agglomerate at a certain point to decrease their surface-free energy; therefore, sodium citrate was added as a complexing and stabilizing agent after 5 h of reaction time. Citrate is a kosmotropic ion that helps structure water molecules near the headgroup of the surfactant. This strategy results in a solid composed of silver nanoparticles embedded in a polymeric silver citrate matrix that forms a 3D mesh of interconnected fibers. Slow aging of the silver citrate fibers leads to their decomposition, exposing the interconnected spherical silver nanoparticles (Ag HSS). This material showed improved plasmonic properties owing to their extensive interconnection, allowing the formation of "hot spots" between particles (areas in which the electromagnetic field is increased). This enhanced property is highly desired for sensing some molecules at ultra-low concentrations using Surface Enhanced Raman Spectroscopy (SERS). The resulting morphology of the Ag HSS is reminiscent of the shape of the branches of a tree because the branches that are formed have the characteristics of fractal geometry.

SYNTHESIS OF HSS USING ELECTRODEPOSITION

Electrochemical pathways can also be used to obtain fractal growth. For example, silver nanodendrites (**Figure 8A**) have been formed by electrodeposition onto an aluminum plate. In this case, zones with high anisotropy (such as the tips and

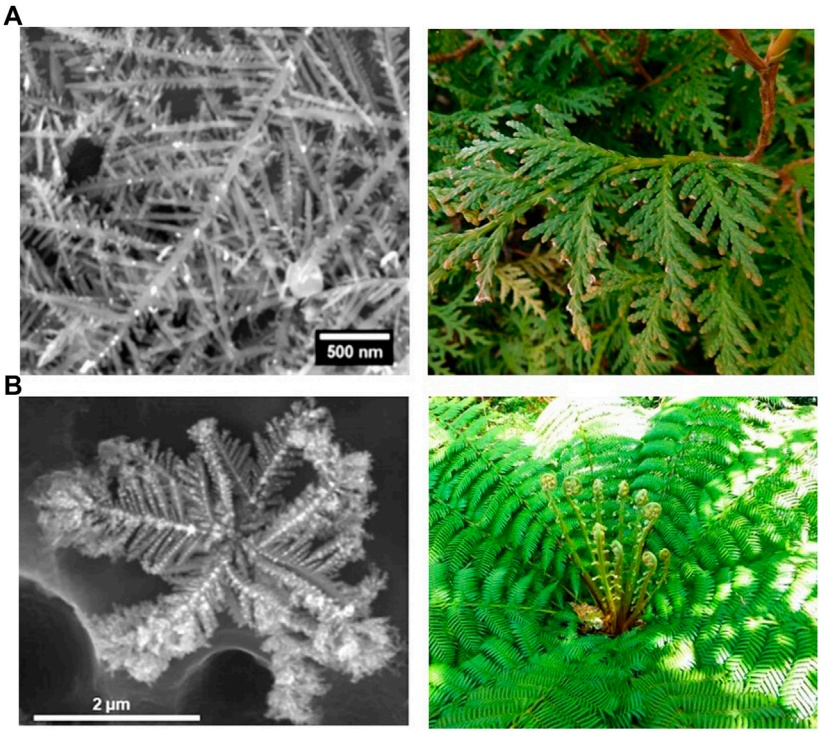

FIGURE 8 | (A) FE-SEM micrograph of silver nanodendrites electrodeposited on aluminum [Reprinted from *Mater. Chem. Phys.* 240 (2020) 122225. Copyright (2020), with permission from Elsevier] compared with the photograph of leaves of the conifer Tuya *(Thuja occidentalis)* (Pixabay license for the public domain. Available on: https://pixabay.com/sv/photos/thuja-cypressv%c3%a4xter-livets-tr%c3%a4d-1571074/). **(B)** SEM micrograph of Ag-Cu bimetallic nanodendrites (Reprinted from Rubén Darío Rivera-Rangel et al. 2020 *Nanotechnology* 31 465605. © 2020 IOP Publishing Ltd.) compared to western swordfern *(Polystichum munitum)* photography (Pixabay license for the public domain. Available on: https://pixabay.com/de/photos/farn-pflanze-farnwedel-ausrollen-123535/).

intersections in nanodendrites) also allow zones with increased electromagnetic fields for SERS applications. In the synthetic method Ceballos et al. (2020), reported silver nanodendrites were grown onto an aluminum alloy 5052-H32 in a two-electrode electrodeposition cell. The electrodes were vertically aligned at a 1 cm distance, using a silver wire as a sacrificial anode. By applying a constant voltage of 5 V for 10 s in an electrolytic solution of $AgNO_3$, silver nanodendrites were obtained; these structures presented a remarkable plasmonic response for detecting a widely used biomarker (Rhodamine 6G). The morphology of silver nanodendrites resembles the foliage of *Thuja occidentalis*, which presents scaly branches.

The electrochemical synthesis also allows the formation of bimetallic nanodendrites, which results in improved optical properties because it extends the absorption region at which the surface plasmons resonate with the incident radiation to the near-infrared region, which is helpful for their application as SERS substrates, making multimetallic SERS substrates very versatile for working under different incident wavelengths. **Figure 8B** shows bimetallic plasmonic nanodendrites of Ag-Cu. Synthesis was described by Rivera-Rangel et al. (2020); a custom-made cell was used for electrodeposition. A piece of 2.5 cm^2 aluminum alloy 5052-H32 plate was used as the substrate (cathode) for electrodeposition; the Microstar DuPr10-3-6 equipment was used as the power source. Ag-Cu bimetallic nanodendrites were obtained by applying a constant potential of 5 V for 60 s using an electrolytic solution composed of silver nitrate and copper nitrate ($AgNO_3$ + Cu $(NO_3)_2$). The resulting morphology reminds us of the shape of the western swordfern *(Polystichum munitum)* leaves and how they grow as they unwind. Ferns are one of the most common plants worldwide. It grows from the sub-Arctic to southern America and Africa with terrestrial and aquatic subspecies characterized by large leaves with circinate prefoliation (Alonso-Amelot, 1999).

Electrochemical techniques offer an undeniable advantage over other techniques for synthesizing metallic HSS, such as a short processing time, and in many cases, biomimetic materials are obtained (Ren et al., 2006; Jiang et al., 2017; Liu et al., 2017; Galvão et al., 2019; Martínez-Cartagena et al., 2021). There are many examples of hard templates for the electrodeposition of three-dimensionally ordered metals. Some excellent examples are the hierarchical structures of silver and palladium-nickel nanowires shown in **Figures 9A,B**, respectively. The synthesis of silver nanowires was described by Strukova et al. (2013), where metal mesostructures were prepared in porous membranes by pulsed current electroplating using a simple scheme of two electrodes using aluminum oxide membranes as porous templates. The membranes were covered with a copper layer from 50 to 100 nm, which served as the cathode, while a platinum foil was used as the anode. The cathode and anode were electrically connected to the pulsed current generator and placed in a bath with the electrolyte to

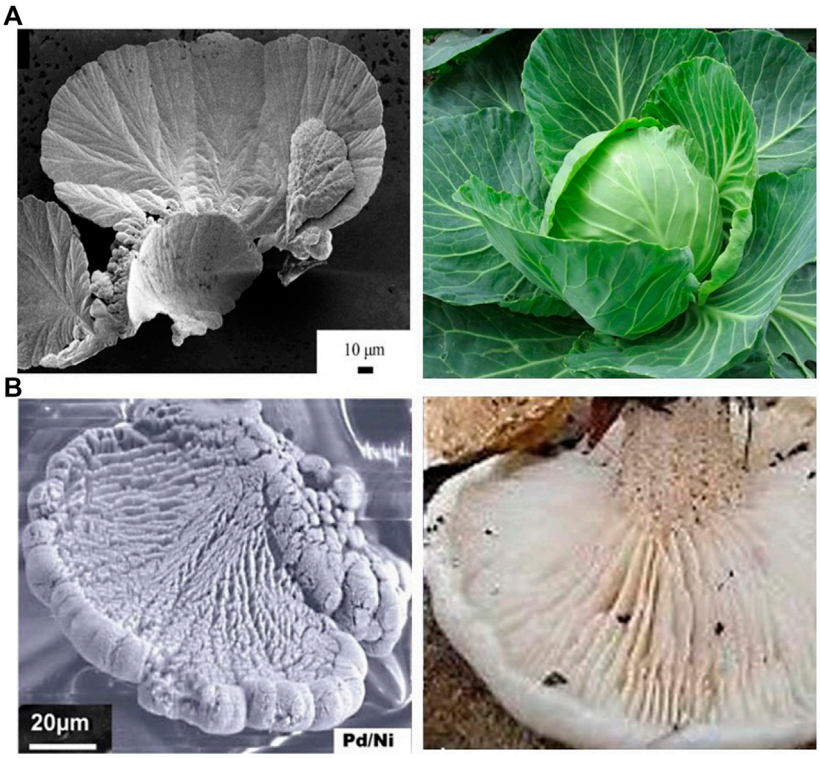

FIGURE 9 | (A) SEM image of electrodeposited silver HSS using Al_2O_3 as a porous template (Reprinted with permission of MRS Proc. 1498 (2013) 183–188. Copyright© Materials Research Society 2013) as compared to a Cabbage leaf *(Brassica oleracea var. capitata)* (CC0 license for Public Domain. Available on: https://pixy.org/5824507/) **(B)** SEM image of a hierarchical Pd-Ni alloy *versus* the photograph of the fruiting body of a fungus (Reprinted with permission of MRS Proc. 1498 (2013) 183–188. Copyright© Materials Research Society 2013).

undergo a cycle of current pulses. The electrolyte for silver electroplating was composed of silver nitrate $AgNO_3$, sulfosalicylic acid, and ammonia. The electroplating was carried out at 20–25°C, resulting in these silver nanowires. This concave-convex structure is reminiscent of cabbage leaves (cabbage or *Brassica oleracea* var. *capitata*), with thick leaves wrapped in the form of a nucleus. The Pd-Ni alloy was obtained using an equivalent strategy (Strukova et al., 2014). In this case, the cathode was a brass net covered with a polymeric porous membrane, and the anode was a Pt plate. The aqueous electrolyte solution was palladium chloride ($PdCl_2$), nickel chloride hexahydrate ($NiCl_2{\cdot}6\ H_2O$), ammonium sulfate, and sodium nitrite. The amplitude of the rectangular current pulse was 100 mA, the duty cycle of the pulse was 50%, the pulse frequency was 100 Hz, and the deposition time was 600–1000 s. The resulting Pd/Ni samples had a laminar architecture similar to that of mushrooms, which are the fruiting bodies of mycelium (fungi).

Electrochemical routes are preferred for obtaining metallic HSS over ceramic or polymeric materials. However, one of the most exciting approaches has been reported as an attempt to obtain artificial nacre by electrophoretic deposition (EDP). Nacre (mother-of-pearl) is an outstanding example of a hierarchical material growing from nano to macroscale, showing an unprecedented high strength. It is well known that the basic structural units of nacre are aragonite biocrystals with a tablet-like shape. The surface of these structures is formed by self-assembled nanoparticles exhibiting sizes ranging from 5–50 nm to 20–180 nm, depending on the formation of spherical or pseudo-hexagonal structures, respectively. The tablet-like shapes show diameters of around 200 nm, which corresponds to the mesoscale. Furthermore, these inorganic tablets assemble up to the microscale (or even at higher scales in some species), forming a composite with some biopolymers (Gao et al., 2019). The SEM image on the left in **Figure 10** shows a composite containing 5 *(wt%)* of a polymer and 95 *(wt%)* of ceramic material (as in natural nacre) prepared by EPD, starting from an acrylamide–modified montmorillonite (MMT) aqueous suspension. The monomer was polymerized under UV light in the presence of MMT clay to yield a multilayered composite (Long et al., 2007). Compared to the SEM image on the left corresponding to the nacreous layer (cross-section) of the donkey's ear abalone, the columnar superimposition characteristic of gastropod nacre illustrates the similarity between both structures.

SYNTHESIS OF HSS COMBINING BμE AND ELECTRODEPOSITION

All the examples above reveal the possibility of combining the advantages of soft templates with electrodeposition to optimize HSS synthesis. However, this option has scarcely been studied,

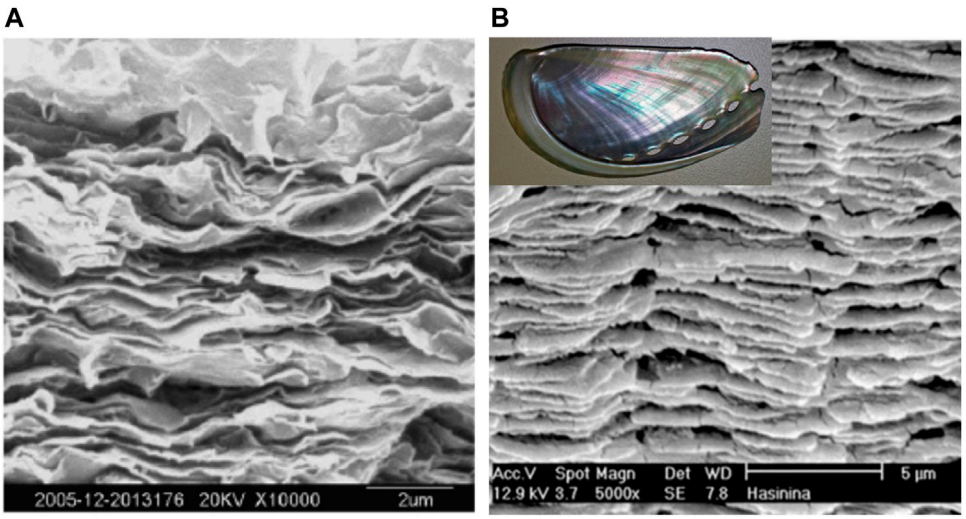

FIGURE 10 | (A) A cross-section of the MMT/polyacrylamide multilayer structure deposited by EPD (Reprinted from Polyacrylamide-clay nacre-like nanocomposites prepared by electrophoretic deposition. Compos. Sci. Technol. 67, 2770–2774 (2007) with permission from Elsevier), **(B)** SEM micrograph of the nacreous layer of the cross-section in *Haliotis asinina* illustrating the columnar superimposition of nacre tablets that is characteristic of gastropod nacre (Copyright © 2010, Marie et al.; licensee BioMed Central Ltd.). Inset: "*Haliotis asinina* (donkey's ear abalone) 3" by James St. John is licensed under CC BY 2.0. Available on: https://commons.wikimedia.org/wiki/File:Haliotis_asinina_(donkey%27s_ear_abalone)_3_(24222578015).jpg.

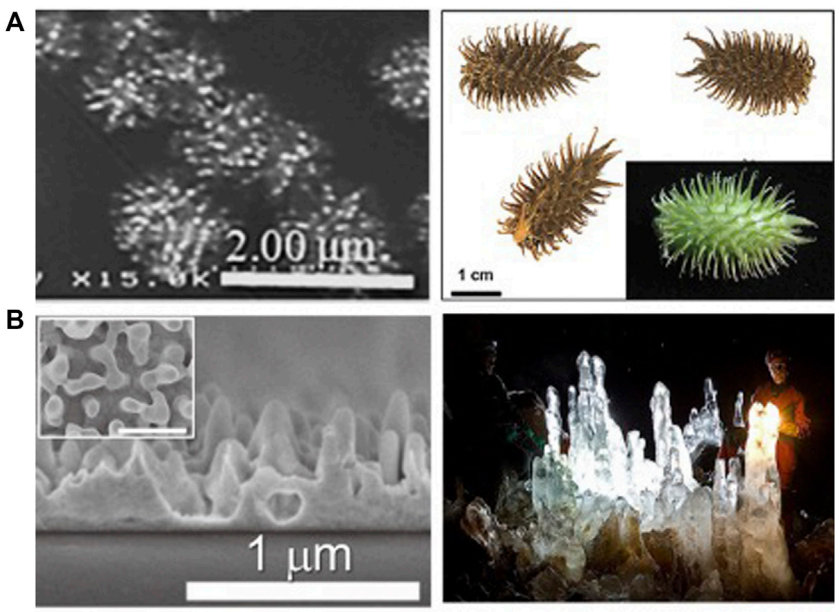

FIGURE 11 | (A)FE-SEM micrograph of the CoNi deposit after circulating –720 mC cm^{-2} of charge density on the material prepared at –300 mC cm^{-2} using a bicontinuous microemulsion as a template (13.5 wt% W, 54.5 wt% O, and 32.0 wt% S) [Reprinted from Microemulsions for obtaining nanostructures through electrodeposition method. Electrochem. Commun. 27, 14–18 (2013) with permission from Elsevier]. *Xanthium strumarium* L. This file is licensed under the Creative Commons Attribution-Share Alike 3.0 Unported license. Available on: https://commons.wikimedia.org/wiki/File:Xanthium_strumarium_MHNT.BOT.2004.0.213.jpg. **(B)** Cross-sectional FE-SEM image of the sputtered Au films after Au electrodeposition in water-rich BµE at –0.30 V. The inset shows the top image of the same section. [Reprinted from Monolithic Au Nanoscale Films with Tunable Nanoporosity Prepared via Dynamic Soft Templating for Electrocatalytic Oxidation of Methanol. ACS Appl. Nano Mater. 3, 7750–7760 (2020) Copyright © 2020, American Chemical Society]. Image of a stalagmite captured at the Búri Cave created by a raging river of lava in Iceland. (CC0 license for Public Domain. Available on: https://www.atlasobscura.com/places/buri).

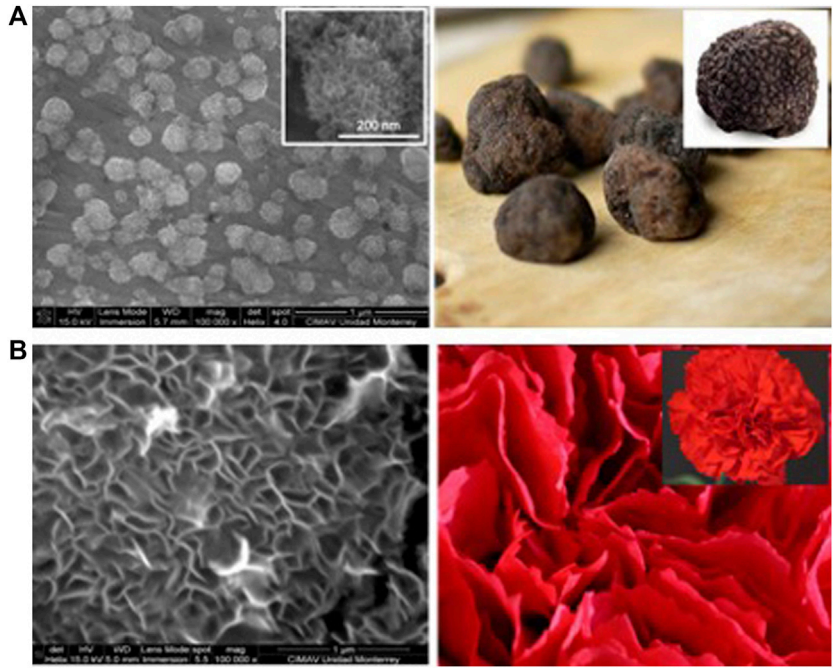

FIGURE 12 | (A) SEM image of electrodeposited Pt hierarchical superstructures onto a glassy carbon electrode using an LSV approach. This image corresponds to an unpublished image from the authors. The obtained structures resemble the truffles *(Tuber melanosporum)* structures as shown in the photographs on the right. "Black Truffles" by ulterior epicure is licensed under CC BY-NC-ND 2.0. Available on: https://www.flickr.com/photos/13329406@N00/370974435. **(B)** SEM image of the NiCo alloy deposited onto an Au electrode, unpublished results from the authors. The wrinkled structure of the NiCo sheets resembles the distribution of the petals in carnation *(Dianthus caryophyllus)* flowers. "Red carnation for mother" by koizumi is licensed under CC BY-NC-ND 2.0. Available on: https://www.flickr.com/photos/59959574@N00/497080969

opening a new niche for synthesizing biomimetic hierarchical materials. The first attempts found in the literature have been reported by Serrà et al. (2013a, 2013b, 2014b, 2014a); Serrà and Vallés, (2018). They performed rapid electrodeposition at high deposition rates in BμE containing high concentrations of metal ions without a supporting electrolyte because of the relatively high conductivity of the solution. This rapid electrodeposition process can replicate the structure of BμE; however, other conditions should be considered to obtain the template effect. Some of these conditions are (1) immiscibility of oil and aqueous solution components, (2) low dielectric constant of the oil to favor the non-dissolution of the electroactive species, and (3) use of a surfactant that avoids the solubilization of electroactive species (Serrà et al., 2014a). For example, a NiCo bimetallic structure was electrodeposited onto a Si/Ti (10 nm)/Au (50 nm) slide using as template a BμE composed of an aqueous solution (0.2 M $CoCl_2$ + 0.9 M $NiCl_2$ + 30 g L^{-1} boric acid +0.7 g L^{-1} saccharin, pH = 3.0) as aqueous phase (13.5 *wt*%), diisopropyl adipate as oil phase (54.5 *wt*%) and Triton X-100 as surfactant (32 *wt*%) (Serrà et al., 2013b). As presented in **Figure 11A**, these structures resemble the fruit of the Asteraceae, *Xanthium strumarium* L. *Xanthium* L. is a genus of the subtribe Ambrosiinae (Heliantheae, Asteraceae), represented by annual herbaceous plants, often found growing in moist sandy pits, riverbanks, and coastal dunes, and are now expanded to open environments created by men, such as cultivated fields, railway embankments, and ruderal places. The fruit has an ellipsoid shape 1.5–2.3 cm long and is covered in hooked spines 3–4 mm long (Tomasello, 2018).

Recently, Shiba et al. (2020) reported the synthesis of monolithic nanoporous gold thin films onto a polished Au disk electrode (−0.30 V, 300 s, scan rate 5 mV s^{-1}). BμE was composed of cyclohexane (oil phase), 50 mM $HAuCl_4$, 1 M HCl (aqueous phase), and a mixture of sodium dodecyl sulfate (SDS) and 2-methyl-2-butanol as the surfactant and co-surfactant, respectively. Based on the current values, they found that diffusion-controlled electrodeposition was similar in water-rich and equally mixed BμEs; however, the apparent diffusion coefficients of $AuCl_4^-$ and H_3O^+ become slow because of the narrow aqueous channels in the oil-rich BμE. The nanoporous structure with a pore size of 40–200 nm was tuned by controlling the composition of the BμE solution. Electrodeposition conditions could control the resultant length of the monolithic structure growing vertically from the electrode surface. As compared in **Figure 11B**, this monolithic structure obtained by a slow deposition rate resembles the formation of stalagmites, a type of rock formation that rises from the floor of a cave owing to the accumulation of material deposited on the floor from ceiling drippings. This is a slow process in which each successive drop adds a thin layer of minerals to a growing stalagmite. As in the electrochemical reactions, the mass diffusion rate and temperature determine the shape of the deposited structures. Therefore, a slow deposition rate could be used for the first deposited nuclei (from the water nanochannels) to develop these monolithic Au nanostructures.

Finally, **Figure 12** shows two approaches of our research group using the BμE composed of isooctane, synperonic 91/5, and water for the electrodeposition of Pt and a NiCo alloy. A nonionic surfactant could be more suitable because it is less susceptible to ionic strength changes during the electrodeposition process. Linear sweep voltammetry (LSV) was used in both cases; the formulation of the microemulsions followed the composition used in the works by Adesuji et al. (2020b), using water-soluble precursors only. Platinum hierarchical superstructures were electrodeposited onto a glassy carbon electrode at a potential of −0.7 to −0.9 V vs. Pt wire and a scan rate of 2 mV/s. Likewise, NiCo material was obtained by applying a 1 mV/s scan rate for a potential range of −1.7 to −0.7 V using a gold slide as a working electrode and a $Hg/HgSO_4$ as the reference electrode. In **Figure 12A**, it could be observed that the porous spherical Pt structures deposited using this strategy resemble the fruiting body of a subterranean ascomycete fungus, also known as a truffle *(Tuber melanosporum).* Truffles are ectomycorrhizal fungi; therefore, they are usually associated with tree roots, meaning they cannot survive in soil without their plant hosts. Mutualistic ectomycorrhizal fungi such as truffles provide valuable nutrients to plants in exchange for carbohydrates (Læssøe and Hansen, 2007). The morphology of the truffle is templated by the texture of the land where it has grown, and its structural features are polygonal projections of 3–5 mm in height. In contrast, the wrinkled structure of the NiCo alloy resembled the petals of the carnation flower (**Figure 12B**). The carnation (Dianthus caryophyllus) is native to the Mediterranean region. It is widely cultivated because of its extensive use in the floral industry. The petals had a complex morphology with two distinct domains. The standard carnation's blade and claw petal area seemed to follow a bimodal distribution, suggesting a mixture of subpopulations of different sizes (Chacón et al., 2013).

CONCLUDING REMARKS

Bicontinuous microemulsions function as confined nanoreactors and soft templates that can give rise to three-dimensional interconnected structures of different chemical nature. Electrochemical routes give rise to hierarchical metal superstructures over short periods of time. Both approaches provide 3D networks (hierarchical systems) and porous fractal branching, which are of great interest for multiple applications, such as adsorption, catalysis, electrocatalysis, and detection. The manipulation of the architecture offers exciting perspectives for preparing novel materials with specific physical properties. The similarity of superstructures with biological objects and metallic, polymeric, and ceramic models exhibits a hierarchical structure typical of natural bodies. We believe that the resemblance of the synthesized structures to nature is not coincidental. This can be explained by some essential mechanisms associated to the nucleation and growth processes and formation of biological structures and tissues, either by their spatial orientation or directed growth, mediated by the nonlinear coupling of factors such as pressure, pH, and concentration of oxygen or carbon dioxide. Another critical aspect of this relationship is the presence of templates or membranes in both cases. Growth usually begins with nuclei that self-assemble in confined spaces, forming fractal ramifications. This analogy offers exciting opportunities to investigate new bio-inspired materials that are reproducible and efficient with a large surface area and controlled architecture.

AUTHOR CONTRIBUTIONS

AS-M, KF, and MS-D gathered bibliography, wrote parts of the manuscript and revised the submitted version; EA and FA performed experiments reported as unpublished results (it is part of their Ph.D. and M.Sc. thesis, respectively) and wrote some parts of the manuscript; VOT-G, EG-V, and KB-B wrote some parts of the manuscript as part of their bachelor thesis; MC, MN-S, and RDR-R perfomed the electrosynthesis of some of the materials and participate in the revision of the manuscript; JA-Z performed SEM of the experiments reported as unpublished results and wrote some parts of the manuscript; MV wrote parts of the manuscript and revised the submitted version.

ACKNOWLEDGMENTS

We are grateful to CONACYT for their financial support (Fronteras de la Ciencia Project: FC 2016/1700, including postdoctoral research stay for KF, and undergraduate research stay for VT, EG-V, and KB). EA and MN-S acknowledge CONACYT for PhD. Grants. FA and MC acknowledge CONACYT for the M.Sc. Grants and RR for postdoctoral grants. We also acknowledge NaNoTeCh from the National Nanotechnology Laboratory of Mexico.

REFERENCES

Adesuji, E. T., Guardado-Villegas, E., Fuentes, K. M., Sánchez-Domínguez, M., and Videa, M. (2020a). Pt-Co_3O_4 Superstructures by One-Pot Reduction/Precipitation in Bicontinuous Microemulsion for Electrocatalytic Oxygen Evolution Reaction. *Catalysts* 10, 1311. doi:10.3390/catal10111311

Adesuji, E. T., Khalil-Cruz, L. E., Videa, M., and Sánchez-Domínguez, M. (2020b). From Nano to Macro: Hierarchical Platinum Superstructures Synthesized Using Bicontinuous Microemulsion for Hydrogen Evolution Reaction. *Electrochimica Acta* 354, 136608. doi:10.1016/j.electacta.2020.136608

Adesuji, E. T., Torres-Guerrero, V. O., Arizpe-Zapata, J. A., Videa, M., Sánchez-Domínguez, M., and Fuentes, K. M. (2020c). Bicontinuous Microemulsion as Confined Reaction Media for the Synthesis of Plasmonic Silver Self-Assembled Hierarchical Superstructures. *Nanotechnology* 31, 425601. doi:10.1088/1361-6528/ab9f75

Alonso-Amelot, Miguel. E. (1999). Braken Fern, Animal and Human Health. *Rev. Fac. Agron.* 16, 528–541.

Amstad, E., and Harrington, M. J. (2021). From Vesicles to Materials: Bioinspired Strategies for Fabricating Hierarchically Structured Soft Matter. *Phil. Trans. R. Soc. A* 379, 20200338. doi:10.1098/rsta.2020.0338

Attard, G. S., Bartlett, P. N., Coleman, N. R. B., Elliott, J. M., Owen, J. R., and Wang, J. H. (1997). Mesoporous Platinum Films from Lyotropic Liquid Crystalline Phases. *Science* 278, 838–840. doi:10.1126/science.278.5339.838

Bates, F. S., Maurer, W. W., Lipic, P. M., Hillmyer, M. A., Almdal, K., Mortensen, K., et al. (1997). Polymeric Bicontinuous Microemulsions. *Phys. Rev. Lett.* 79, 849–852. doi:10.1103/PhysRevLett.79.849

Belegratis, M. R., Schmidt, V., Nees, D., Stadlober, B., and Hartmann, P. (2013). Diatom-inspired Templates for 3D Replication: Natural Diatoms versus Laser Written Artificial Diatoms. *Bioinspir. Biomim.* 9, 016004. doi:10.1088/1748-3182/9/1/016004

Brodie, J., Ingham, C. J., and Vignolini, S. (2021). Does Structural Color Exist in True Fungi? *JoF* 7, 141. doi:10.3390/jof7020141

Ceballos, M., Arizmendi-Morquecho, A., Sánchez-Domínguez, M., and López, I. (2020). Electrochemical Growth of Silver Nanodendrites on Aluminum and Their Application as Surface-Enhanced Raman Spectroscopy (SERS) Substrates. *Mater. Chem. Phys.* 240, 122225. doi:10.1016/j.matchemphys.2019.122225

Chacón, B., Ballester, R., Birlanga, V., Rolland-Lagan, A.-G., and Pérez-Pérez, J. M. (2013). A Quantitative Framework for Flower Phenotyping in Cultivated Carnation (Dianthus Caryophyllus L.). *PLoS One* 8, e82165. doi:10.1371/journal.pone.0082165

Chew, C. H., Li, T. D., Gan, L. H., Quek, C. H., and Gan, L. M. (1998). Bicontinuous-Nanostructured Polymeric Materials from Microemulsion Polymerization. *Langmuir* 14, 6068–6076. doi:10.1021/la970990a

Coral Reef Alliance (2021). CORAL POLYPS — TINY BUILDERS. Available at: https://coral.org/coral-reefs-101/coral-reef-ecology/coral-polyps/(Accessed August 18, 2021).

Danielsson, I., and Lindman, B. (1981). The Definition of Microemulsion. *Colloids Surfaces* 3, 391–392. doi:10.1016/0166-6622(81)80064-9

Dobrovolska, T., López-Sauri, D. A., Veleva, L., and Krastev, I. (2012). Oscillations and Spatio-Temporal Structures during Electrodeposition of AgCd Alloys. *Electrochimica Acta* 79, 162–169. doi:10.1016/j.electacta.2012.06.100

Fradin, C., Orange, F., Amigoni, S., Guittard, F., and Darmanin, T. (2022). Effect of Electrolyte Nature on Micellar Soft-Template Electropolymerization in Organic Solvent to Form Nanoporous Polymer Films with a Bioinspired Strategy. *J. Bionic Eng.* 19, 547–553. doi:10.1007/s42235-021-00131-7

Fuentes, K. M., Coria-Oriundo, L. L., Wirth, S., and Bilmes, S. A. (2020). Functionalized Hierarchical Wrinkled-Silica Spheres for Laccases Immobilization. *J. Porous Mat.* 28, 261–269. doi:10.1007/s10934-020-00988-9

Fuentes, K. M., Sánchez-Dominguez, M., and Bilmes, A. (2019). "TiO_2 Nanoparticles Supported on Hierarchical Meso/Macroporous SiO_2 Spheres for Photocatalytic Applications," in *Concepts of Semiconductor Photocatalysis* (London: IntechOpen). doi:10.5772/intechopen.86153

Galiano, F., André Schmidt, S., Ye, X., Kumar, R., Mancuso, R., Curcio, E., et al. (2018). UV-LED Induced Bicontinuous Microemulsions Polymerisation for Surface Modification of Commercial Membranes - Enhancing the Antifouling Properties. *Sep. Purif. Technol.* 194, 149–160. doi:10.1016/j.seppur.2017.10.063

Galvão, R. A., Santa-Cruz, L. A. d., Barreto, P. B., Horta, M. K. D. S., Andrade, A. M. H. d., Moura, F. J., et al. (2019). Electrochemical Single-step Obtention and Characterization of a Biomimetic TiO_2-HA NTs Covered by Chitosan. *J. Mat. Res.* 34, 1868–1878. doi:10.1557/jmr.2019.23

Gao, R., Wang, R., Feng, X., and Zhang, G. (2019). Growth of Nacre Biocrystals by Self-Assembly of Aragonite Nanoparticles with Novel Subhedral Morphology. *Crystals* 10, 3. doi:10.3390/cryst10010003

Guevara-Chumacero, I. C. R.-G. L. M. (2006). Variation in the Colour and Fur Patterns in Felines. *Investig. Cienc.* 25, 94–101. Available at: https://www.redalyc.org/journal/674/67452917012/html/.

Holmberg, K. (2004). Surfactant-templated Nanomaterials Synthesis. *J. Colloid Interface Sci.* 274, 355–364. doi:10.1016/j.jcis.2004.04.006

Iqbal, P., Preece, J. A., and Mendes, P. M. (2012). "Nanotechnology: The 'Top-Down' and 'Bottom-Up' Approaches," in *Supramolecular Chemistry* (Chichester, UK: John Wiley & Sons, Ltd). doi:10.1002/9780470661345.smc195

Jiang, S., Guo, Z., Liu, G., Gyimah, G. K., Li, X., and Dong, H. (2017). A Rapid One-step Process for Fabrication of Biomimetic Superhydrophobic Surfaces by Pulse Electrodeposition. *Mater. (Basel)* 10. doi:10.3390/ma10111229

Jones, B. H., and Lodge, T. P. (2010). Nanoporous Materials Derived from Polymeric Bicontinuous Microemulsions. *Chem. Mat.* 22, 1279–1281. doi:10.1021/cm903408x

Judit, H., István, S., and Patrick, D. K. (2009). An Experimental Design Method Leading to Chemical Turing Patterns. *Sci. (80-.)* 324, 772–775. doi:10.1126/science.1169973

Kawamura, G., Muto, H., and Matsuda, A. (2014). Hard Template Synthesis of Metal Nanowires. *Front. Chem.* 2. doi:10.3389/fchem.2014.00104

Læssøe, T., and Hansen, K. (2007). Truffle Trouble: what Happened to the Tuberales? *Mycol. Res.* 111, 1075–1099. doi:10.1016/j.mycres.2007.08.004

Latsuzbaia, R., Negro, E., and Koper, G. (2015). Bicontinuous Microemulsions for High Yield, Wet Synthesis of Ultrafine Nanoparticles: a General Approach. *Faraday Discuss.* 181, 37–48. doi:10.1039/C5FD00004A

Le Roy, N., Ganot, P., Aranda, M., Allemand, D., and Tambutté, S. (2021). The Skeletome of the Red Coral Corallium Rubrum Indicates an Independent Evolution of Biomineralization Process in Octocorals. *BMC Ecol. Evol.* 21, 1. doi:10.1186/s12862-020-01734-0

Leblanc, J. (2019). The Desert Roses And Other Recent Gypsum Crystals Of Qatar. Available at: https://sites.google.com/site/leblancjacques/fossilhome.

Li, C., Iqbal, M., Lin, J., Luo, X., Jiang, B., Malgras, V., et al. (2018). Electrochemical Deposition: An Advanced Approach for Templated Synthesis of Nanoporous Metal Architectures. *Acc. Chem. Res.* 51, 1764–1773. doi:10.1021/acs.accounts.8b00119

Lindman, B., Shinoda, K., Olsson, U., Anderson, D., Karlström, G., and Wennerström, H. (1989). On the Demonstration of Bicontinuous Structures in Microemulsions. *Colloids Surfaces* 38, 205–224. doi:10.1016/0166-6622(89)80154-4

Liu, Y., Xue, J., Luo, D., Wang, H., Gong, X., Han, Z., et al. (2017). *One-step Fabrication of Biomimetic Superhydrophobic Surface by Electrodeposition on Magnesium Alloy and its Corrosion Inhibition*. Elsevier. doi:10.1016/j.jcis.2016.12.022

Long, B., Wang, C.-A., Lin, W., Huang, Y., and Sun, J. (2007). Polyacrylamide-clay Nacre-like Nanocomposites Prepared by Electrophoretic Deposition. *Compos. Sci. Technol.* 67, 2770–2774. doi:10.1016/j.compscitech.2007.02.007

Martínez-Cartagena, M. E., Bernal-Martínez, J., Aranda-Sánchez, C. A., Banda-Villanueva, A., Gonzalez-Zapata, J. L., Ledezma-Pérez, A., et al. (2021). Biomimetic Synthesized Conductive Copolymer EDOT-Pyrrole Electrodes for Electrocardiogram Recording in Humans. *J. Mat. Sci. Chem. Eng.* 09, 19–40. doi:10.4236/msce.2021.910003

Mason, C. W. (1926). Structural Colors in Insects. I. *J. Phys. Chem.* 30, 383–395. doi:10.1021/j150261a009

Mason, C. W. (1927). Structural Colors in Insects. II. *J. Phys. Chem.* 31, 321–354. doi:10.1021/j150273a001

Mercatelli, R., Mattana, S., Capozzoli, L., Ratto, F., Rossi, F., Pini, R., et al. (2019). Morpho-mechanics of Human Collagen Superstructures Revealed by All-Optical Correlative Micro-spectroscopies. *Commun. Biol.* 2, 117. doi:10.1038/s42003-019-0357-y

Miguez, H., López, C., Meseguer, F., Blanco, A., Vázquez, L., Mayoral, R., et al. (1997). Photonic Crystal Properties of Packed Submicrometric SiO2 Spheres. *Appl. Phys. Lett.* 71, 1148–1150. doi:10.1063/1.119849

Moon, D.-S., and Lee, J.-K. (2012). Tunable Synthesis of Hierarchical Mesoporous Silica Nanoparticles with Radial Wrinkle Structure. *Langmuir* 28, 12341–12347. doi:10.1021/la302145j

Newman, H. H. (1944). Finger Prints, Palms and Soles: An Introduction to Dermatoglyphics. *Am. J. Phys. Anthropol.* 2, 227–229. doi:10.1002/ajpa.1330020212

Notar Francesco, I., Fontaine-Vive, F., and Antoniotti, S. (2014). Synergy in the Catalytic Activity of Bimetallic Nanoparticles and New Synthetic Methods for the Preparation of Fine Chemicals. *ChemCatChem* 6, 2784–2791. doi:10.1002/cctc.201402252

Olsson, U., and Lindman, B. (1990). "Uni- and Bicontinuous Microemulsions," in *The Structure, Dynamics and Equilibrium Properties of Colloidal Systems* (Dordrecht: Springer Netherlands), 233–242. doi:10.1007/978-94-011-3746-1_16

Omar, M. A. I. (2021). Electrodeposition of Ni-Co Film: A Review. *Int. J. Electrochem. Sci.* doi:10.20964/2021.01.16

Pemartin, K. L. (2013). *Inorganic Nanoparticles Synthesized by the Novel Oil-In-Water Microemulsion Reaction Method and Their Potential Applications*.

Quintanilla Carvajal, M. X., Arenas Ocampo, M. L., Campos Mendiola, R., Camacho Díaz, B. H., and Jiménez Aparicio, A. R. (2015). Caracterización morfométrica de estructuras florales de Tagetes erecta L. y Tagetes patula L. (Asteraceae) utilizando análisis digital de imágenes y dimensión fractal. *Gayana. Botánica* 72, 137–144. doi:10.4067/S0717-66432015000100016

Ren, L. Q., Liu, Y., Yu, S. R., Han, Z. W., and Hu, H. X. (2006). Preparation, Microstructure and Properties of Biomimetic Nanocomposite Coating. *WIT Trans. Ecol. Environ.* 87, 167–174. doi:10.2495/DN060161

Rivera-Rangel, R. D., Navarro-Segura, M. E., Arizmendi-Morquecho, A., and Sánchez-Domínguez, M. (2020). Electrodeposition of Plasmonic Bimetallic Ag-Cu Nanodendrites and Their Application as Surface-Enhanced Raman Spectroscopy (SERS) Substrates. *Nanotechnology* 31, 465605. doi:10.1088/1361-6528/abacf5

Rosedale, J. H., Bates, F. S., Almdal, K., Mortensen, K., and Wignall, G. D. (1995). Order and Disorder in Symmetric Diblock Copolymer Melts. *Macromolecules* 28, 1429–1443. doi:10.1021/ma00109a014

Sanchez-Dominguez, M., Aubery, C., and Solans, C. (2012). "New Trends on the Synthesis of Inorganic Nanoparticles Using Microemulsions as Confined Reaction Media," in *Smart Nanoparticles Technology* (London: InTech). doi:10.5772/33010

Serrà, A., Gómez, E., Calderó, G., Esquena, J., Solans, C., and Vallés, E. (2014a). Conditions that Bicontinuous Microemulsions Must Fulfill to Be Used as Template for Electrodeposition of Nanostructures. *J. Electroanal. Chem.* 720–721, 101–106. doi:10.1016/j.jelechem.2014.03.033

Serrà, A., Gómez, E., Calderó, G., Esquena, J., Solans, C., and Vallés, E. (2013a). Conductive Microemulsions for Template CoNi Electrodeposition. *Phys. Chem. Chem. Phys.* 15, 14653. doi:10.1039/c3cp52021h

Serrà, A., Gómez, E., Calderó, G., Esquena, J., Solans, C., and Vallés, E. (2013b). Microemulsions for Obtaining Nanostructures by Means of Electrodeposition Method. *Electrochem. Commun.* 27, 14–18. doi:10.1016/j.elecom.2012.10.031

Serrà, A., Gómez, E., and Vallés, E. (2014b). Electrosynthesis Method of CoPt Nanoparticles in Percolated Microemulsions. *RSC Adv.* 4, 34281–34287. doi:10.1039/C4RA03880K

Serrà, A., and Vallés, E. (2018). Microemulsion-Based One-step Electrochemical Fabrication of Mesoporous Catalysts. *Catalysts* 8, 395. doi:10.3390/catal8090395

Sgura, I., Lawless, A. S., and Bozzini, B. (2019). Parameter Estimation for a Morphochemical Reaction-Diffusion Model of Electrochemical Pattern Formation. *Inverse Probl. Sci. Eng.* 27, 618–647. doi:10.1080/17415977.2018.1490278

Shen, J., Min Xie, Y., Huang, X., Zhou, S., and Ruan, D. (2012). Mechanical Properties of luffa Sponge. *J. Mech. Behav. Biomed. Mat.* 15, 141–152. doi:10.1016/j.jmbbm.2012.07.004

Shi, Y., Zhang, M., Zhao, J., Zhang, L., Cui, X., Zhu, X., et al. (2021). Sodium Dodecylbenzene Sulfonate Assisted Electrodeposition of MnO_2 @C Electrode for High Performance Supercapacitor. *J. Electrochem. Soc.* 168, 122502. doi:10.1149/1945-7111/ac41f3

Shiba, S., Hirabayashi, S., Niwa, O., Kato, D., Kunitake, M., and Matsuguchi, M. (2020). Monolithic Au Nanoscale Films with Tunable Nanoporosity Prepared via Dynamic Soft Templating for Electrocatalytic Oxidation of Methanol. *ACS Appl. Nano Mat.* 3, 7750–7760. doi:10.1021/acsanm.0c01316

Sims, S. D., Walsh, D., and Mann, S. (1998). Morphosynthesis of Macroporous Silica Frameworks in Bicontinuous Microemulsions. *Adv. Mat.* 10, 151–154. doi:10.1002/(sici)1521-4095(199801)10:2<151::aid-adma151>3.0.co;2-u

Song, G., Li, J., Yuan, Y., Yao, L., Gu, J., Liu, Q., et al. (2019). Large-Area 3D Hierarchical Superstructures Assembled from Colloidal Nanoparticles. *Small* 15, 1805308. doi:10.1002/smll.201805308

Strukov, G. V., and Strukova, G. K. (2013). Biomimetic Method for Metallic Nanostructured Mesoscopic Models Fabrication. *MRS Proc.* 1498, 183–188. doi:10.1557/opl.2013.334

Strukova, G. K., Strukov, G. V., Egorov, S. V., Mazilkin, A. A., Khodos, I. I., and Vitkalov, S. A. (2014). 3D-mesostructures Obtained by Self-Organization of Metallic Nanowires. *Mat. Lett.* 128, 212–215. doi:10.1016/j.matlet.2014.04.140

Strukova, G. K., Strukov, G. V., Postnova, E. Y., Rusanov, A. Y., and Veshchunov, I. S. (2013). Mesoscopic Models of Plants Composed of Metallic Nanowires. *J. Bionic Eng.* 10, 368–376. doi:10.1016/S1672-6529(13)60232-2

The Editors of Encyclopaedia (2018). Allium. Encycl. Br. Available at: https://www.britannica.com/plant/allium-plant (Accessed August 18, 2021).

Tomasello, S. (2018). How Many Names for a Beloved Genus? Coalescent-Based Species Delimitation in Xanthium L. (Ambrosiinae, Asteraceae). *Mol. Phylogenet. Evol.* 127, 135–145. doi:10.1016/j.ympev.2018.05.024

Torruco Gómez, D., and González Solís, A. (2011). *Estado actual de los corales.* Biodiversidad, 1, 204–208. Available at: https://www.cicy.mx/Documentos/CICY/Sitios/Biodiversidad/pdfs/Cap4/22 Los corales.pdf.

Turing, A. M. (1952). The Chemical Basis of Morphogenesis. *Philos. Trans. R. Soc. Lond. B. Biol. Sci.* 237, 37–72. doi:10.1098/rstb.1952.0012

Walsh, D., and Mann, S. (1996). Chemical Synthesis of Microskeletal Calcium Phosphate in Bicontinuous Microemulsions. *Chem. Mat.* 8, 1944–1953. doi:10.1021/cm9601345

Wang, Y., Li, Y., Ding, L., Tang, Y., and Ding, J. (2021). An (Mn,Ni)O(OH) Turing Structural Nanoscale Film Driving Highly Efficient Urea Oxidization Reaction in Alkali Water, Seawater and Waste Water. *Surf. Coatings Technol.* 408, 126799. doi:10.1016/j.surfcoat.2020.126799

Yang, H., Coombs, N., and Ozin, G. A. (1997). Morphogenesis of Shapes and Surface Patterns in Mesoporous Silica. *Nature* 386, 692–695. doi:10.1038/386692a0

Zeng, F., Sun, Z., Wang, C., Ren, B., Liu, X., and Tong, Z. (2002). Fabrication of Inverse Opal via Ordered Highly Charged Colloidal Spheres. *Langmuir* 18, 9116–9120. doi:10.1021/la020114j

Zhang, J., Ma, J. H., Bai, J., Yang, D., Zhang, M., Yang, Z., et al. (2021). A Facile Template-Assisted Electrodeposition Approach to Porous Cu/Cu_2O Nanowires. *RSC Adv.* 11, 30215–30221. doi:10.1039/D1RA04770A

Zhu, C., Du, D., Eychmüller, A., and Lin, Y. (2015). Engineering Ordered and Nonordered Porous Noble Metal Nanostructures: Synthesis, Assembly, and Their Applications in Electrochemistry. *Chem. Rev.* 115, 8896–8943. doi:10.1021/acs.chemrev.5b00255

Conflict of Interest: The authors declare that the research was conducted in the absence of any commercial or financial relationships that could be construed as a potential conflict of interest.

Publisher's Note: All claims expressed in this article are solely those of the authors and do not necessarily represent those of their affiliated organizations, or those of the publisher, the editors, and the reviewers. Any product that may be evaluated in this article, or claim that may be made by its manufacturer, is not guaranteed or endorsed by the publisher.